Improved method to analyze hyperspectral characteristics of coral reefs

Yang Chaoyu (杨超宇)[1] and Yang Dingtian (杨顶田)[2*]

[1]*South China Sea Marine Prediction Center, State Oceanic Administration, Guangzhou 510301, China*

[2]*State Key Laboratory of Oceanography in the Tropics, South China Sea Institute of Oceanology, Chinese Academy of Sciences, Guangzhou 510301, China*

[*]*Corresponding author: dtyang@scsio.ac.cn*

Received December 24, 2013; accepted March 15, 2014; posted online November 3, 2014

Hyperspectral optimization process exemplar, $a\&b_b$-based K model, and a water column correction model are used to process the hyperspectral data for detecting the subtle spectral difference of coral reefs. The water column correction model only tracks those effective photons by fully considering the geometrical distribution of the light field. The adaptivity of the parameters and models to the in situ data collected in Sanya Bay is evaluated. The modeled and uncorrected spectra are examined separately to reflect the coral reflectance, and the coefficients of determination for the relationships drops from 0.90 to 0.05. The retrieved bottom reflectance for 70 corals (Acropora, Porites) exhibited the classic chlorophyll features. The reflectance at 700 nm collected in Sanya Bay is relatively lower than the results conducted by other researchers. Peak ratio index and derivative analysis are utilized and are proved to be effective for coral reef classification and coral healthy assessment.

OCIS codes: 100.3005, 100.3008, 100.3010.

doi: 10.3788/COL201412.S21001.

Remote sensing techniques are often used to detect the distribution of coral reef. In fact, not only the difference among different substrates but also the subtle difference in hyperspectral reflectance due to different health conditions, different species, even the different habitats need to be identified. For improving the accuracy of the spectral analysis, the water column effects must be removed. Marine remote sensing is quite complex as the signals have to pass through the water column before hitting the sea bottom[1]. The single scattering theory and numerical simulations, which require substantial computational effort per iteration, are often used[2]. Subtracting a deep water reflectance or utilizing the water optical properties that are derived from adjacent deep waters would over sample the deep water spectral space region with similar reflectance spectra produced from unnecessary forward model runs[3]. In order to study the optical characteristics of coral in a local area, bottom reflectance needs to be retrieved to completely reflect the real (bottom) spectra rather than repeating the runs of the forward model with differing parameter values and searching a similar spectra by pre-calculation of reflectance optionally with interpolation across tabulated points if complete hyperspectral library is lacking. By considering the interaction between multiple parameters and the bottom reflectance, an optical model of in-coming solar radiation transfer was applied to correct the water column effects.

Field study was conducted in April 2011 (109°25′–109°29′E, 18°12′–18°13′N) in Sanya Bay, Hainan, China, with a water surface area of 120 km^2 and an average depth of 16 m[4]. A self-designed remote cosine receptor was connected to the spectrometer (S2000, Oceanoptics, Inc.) with a multi-mode step index optical fiber (P400-2-UV/VIS). A 30-m underwater optical cable and 10° field of view (FOV) foreoptic were used to measure submerged features during scuba diving. The spectral scan limits of the instrument are 200 and 1100 nm, with a wavelength resolution of 0.3 nm. The sensor was used to measure signals proportional to the sea surface radiance, sky radiance and the radiance reflected from a horizontal reference panel. The relative azimuth measured with respect to the sun azimuth was 135°, and the viewing angle was 40°.

In order to collect the signal directly reflected by the coral, a diver pointed the collecting tip of the fiber optic cable at the desired bottom-type and depressed a button at the end of a 30-m-long trigger cable, prompting the computer to store the spectrum. Immediately thereafter, the diver pointed the collecting tip at a Spectralon diffuse reflectance target (same depth as the target bottom-type) and triggered the storage of its spectrum. The radiometer operator remained above water to take note of sky and water surface conditions and set the integration time.

For the coral living in optically shallow water, the remote sensing reflectance not only depends on the spectral absorption, scattering and fluorescence properties of multiple pigments, including the zooxanthellae and ectodermal and endodermal host tissues, and the structure and geometry of the coral skeleton, but also on the absorption and scattering properties of dissolved and suspended materials in the water column and ocean depth. So, the optical information from

 © 2014 Chinese Optics Letters

water column must be removed from the remote sensing signals for improving the accuracy of hyperspectral analysis of coral reefs. Figure 1 presents the flow chart of the concept of the level by level derivation.

A model-driven spectral optimization technique (hyperspectral optimization process exemplar) developed by Lee *et al.*[5], was used to retrieve the absorption and backscattering coefficients, and water depth from ocean color remote sensing[6].

The attenuation coefficient can be obtained by using a $a\&b_b$-based K model[7].

$$k = (1 + 0.005\theta_\partial)a + 4.18(1 - 0.52\exp(-10.8a))b_b, \quad (1)$$

where θ_∂ is the above surface solar zenith angle in degrees, a is the absorption coefficient, and b_b is backscattering coefficient.

The core of the new method is a water column correction model only tracked those effective photons which can reach the detector by fully considering the geometry distribution of the light field, the solar zenith angle, the path of the scattered photons, the position of the detector and the target, and the FOV of the sensor[8]. The contribution of water column to the subsurface reflectance, $R^w_{rs}(0^-, \lambda)$, can be calculated from the model:

$$R^w_{rs}\left(0^-, \lambda\right) = Q \cdot \left(\frac{\exp\left(-2k\left(H - z_s\right)\right) - 1}{-2k} \right) \cdot \left[-2\pi\beta_w\left(90°, \lambda_0\right) \cdot \left(\frac{\lambda_0}{\lambda} \right)^{4.32} \cdot \left(\cos\Psi + \frac{0.835}{3}\cos^3\Psi \right) - \frac{b_{bp}}{2g} \cdot \frac{1 - g^2}{\left(1 + g^2 - 2g\cos\Psi\right)^{1/2}} \right]\Bigg|_{\psi_1}^{\psi_2}, \quad (2)$$

where Q is the ratio of the subsurface upward irradiance to radiance conversion factor[9], λ is the wavelength, H is water depth measured downward from the detector, z_s is the distance between ocean surface and the detector, and $\beta_w(\psi, \lambda)$ is the total volume scattering function for pure seawater[10], Morel *et al.* gave the values of $\beta_w(90°, \lambda_0)$ at the reference wavelengths of 350 and 600 nm, and λ_0 is the wavelength value selected from the reference wavelength table. The wavelength dependence of $\lambda^{-4.32}$ results from the wavelength dependence of the index of refraction, the factor 0.835 is attributed to the anisotropic properties of the water molecules[11], b_{bp} is the particle backscattering coefficient, and g is a parameter that can be adjusted to control the relative amounts of forward and backward scattering in β_{HG}, the Henyey–Greenstein phase function[12]. In addition, ψ is the angle of reflection of the incident beam, ψ_1 and ψ_2 can be expressed as

$$\psi_1 = -\left(a_0 + \theta_0 + \frac{\text{FOV}}{2}\right) + \pi, \quad (3)$$

$$\psi_2 = -\left(a_0 + \theta_0 + \frac{\text{FOV}}{2}\right) + \pi, \quad (4)$$

where FOV is the field of view of the sensor, α_0 is the solar altitude, and θ_0 is the view angle.

Finally, the coral reflectance can be obtained from subsurface reflectance, the path length in water of light reflected by coral reefs and the well-known Snell's law:

$$R_{rs}^{\text{coral}} = \left(R_{rs}(0^-) - R^w_{rs}(0^-)\right) \exp\left(-\left\{ \left[1 - \left(\frac{\cos a_0}{n} \right)^2 \right]^{-\frac{1}{2}} + \left[1 - \left(\frac{\sin\theta_0}{n} \right)^2 \right]^{-\frac{1}{2}} \right\} kH \right), \quad (5)$$

where n is the refractive index of water.

The predicted value of R^b_{rs} agreed well with the coral reflectance in situ measured Fig. 2, and, the coefficient of determination for the relationship (R^2) was 0.90. In contrast, the relationship between the uncorrected reflectance and coral reflectance is very low ($R^2 = 0.05$, Fig. 3(a)). The uncorrected spectra were similar to that of optically deep water and showed rapid decline at wavelengths longer than 575 nm, attributed to the rapid attenuation of light by water. The first reflection

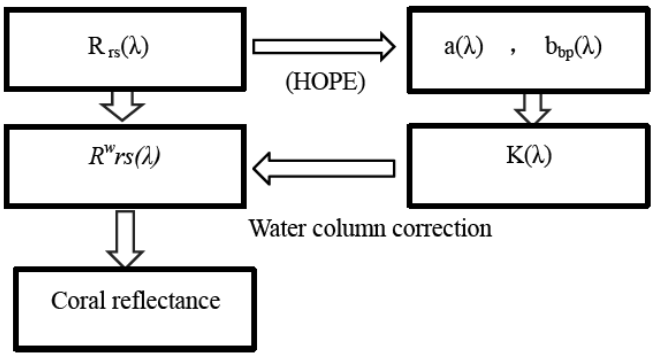

Fig. 1. Flow chart of the algorithm.

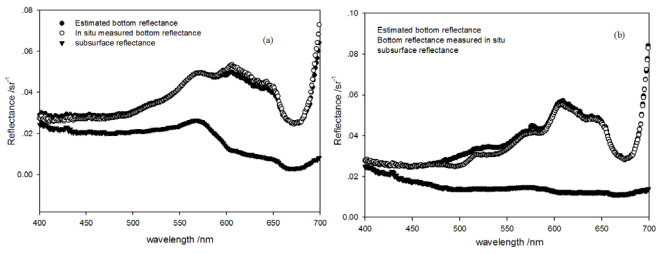

Fig. 2. The reflectance of coral reefs plotted against wavelengths between 400 and 700 nm. The solid dots represent the experimental reflectance values of coral reefs; the hollow dots represent the corresponding values retrieved by the semi-empirical model; the solid triangles represent the in situ measured subsurface reflectance.

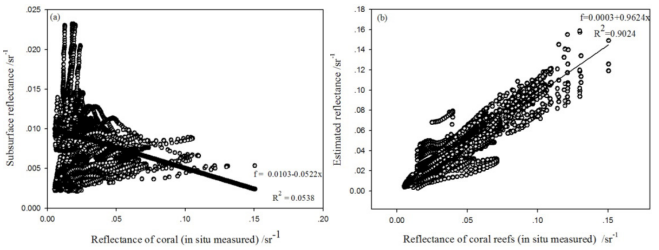

Fig. 3. (a) Comparison of the in situ measured bottom reflectance with subsurface reflectance; *X*-axis shows the reflectance of coral reef measured in Sanya Bay in 2011; *Y*-axis shows the in situ measured subsurface reflectance. (b) The experimental reflectance of coral reefs plotted against the corresponding values retrieved by the semi-empirical model; *X*-axis shows the reflectance of coral reef measured in Sanya Bay in 2011; *Y*-axis shows the bottom reflectance calculated with Eq. (5) following the procedure mentioned in water column correction algorithm section.

peak is located at near 600 nm in the curve of the coral reflectance but at near 550 nm in uncorrected reflectance. The results indicated that the abilities of the hyperspectral remote sensing data to reflect the spectrum of coral reefs and capture the optical properties of coral reefs were limited when the effects of the water column are included. The correlation coefficients for the relationships (R^2) between the modeled and measured coral reflectance and between the uncorrected and coral reflectance dropped from 0.90 to 0.05. The uncorrected spectra contain some information of the water column which results in spectral shifts. Most of the photons are absorbed or scattered by phytoplankton, suspended organic and inorganic matter, and dissolved organic substances. The first reflection peak shift toward short wave suggests an increased absorption of light by chlorophyll. The signals detected from coral surface are relatively weak, while concentration of chlorophyll in water is high. While light penetrates water, its intensity decreases exponentially with increasing depth, thus requires a water column correction. The core of the new method to retrieve the hyperspectral reflectance of coral reef is the water column correction algorithm, which enables us to simulate radiation fields in a wide range of optical characteristics of these layers to analyze the mechanisms of the formation of the radiation characteristics inside and outside the layers, and to estimate any contribution of each region. Only those effective photons which can reach the detector were tracked by fully considering the geometry distribution of the light field, the solar zenith angle, the path of the scattered photons, the position of the detector and the target, and the FOV of the sensor. The particle phase function can be changed according to the composition and spatial distribution of particle size in ocean water for further improving the efficiency of the model in different areas. Based on the validation by using the in situ hyperspectral data, the model was proved to be effective to capture the optical properties of coral reefs during the whole band. The subtle difference can be analyzed based on the modeled reflectance. The method is meaningful and necessary before analyzing and establishing the bio-optical models of coral reefs.

Figure 4 shows the overall mean reflectance rise from 0.014 sr^{-1} at 400–500 nm to 0.018 sr^{-1} at 550–650 nm. An obvious shoulder can be observed at near 650 nm with a value of about 0.01 sr^{-1}. A slight drop was observed at near 575 nm in the reflectance spectra governed primarily by the absorption properties of pure sea water. The upwelling radiance above water exhibits similarities to optically deep water, although differences exist in magnitude, which illustrates that the water leaving signals are modified by absorption and scattering properties of shallow water. Hyperspectral reflectance for 70 corals (Acropora, Porites) was retrieved (Fig. 5), which exhibited the classic chlorophyll features with lower values in blue and green spectral region due to the strong absorption of photosynthetic pigments, with higher values at longer wavelengths corresponding

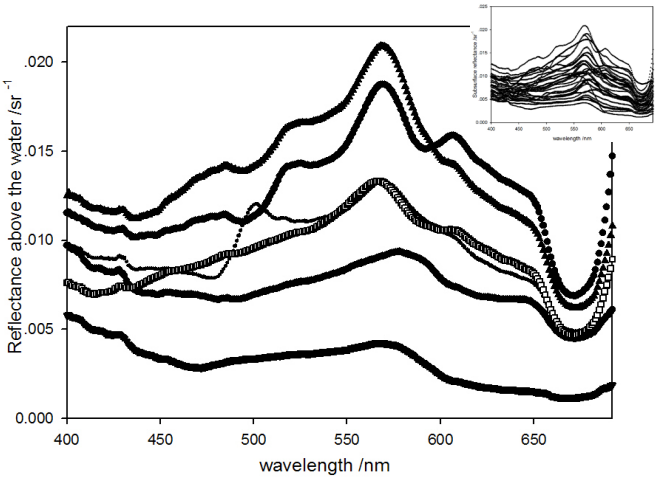

Fig. 4. In situ measured reflectance above the water in Sanya plotted against wavelength between 400 and 700 nm.

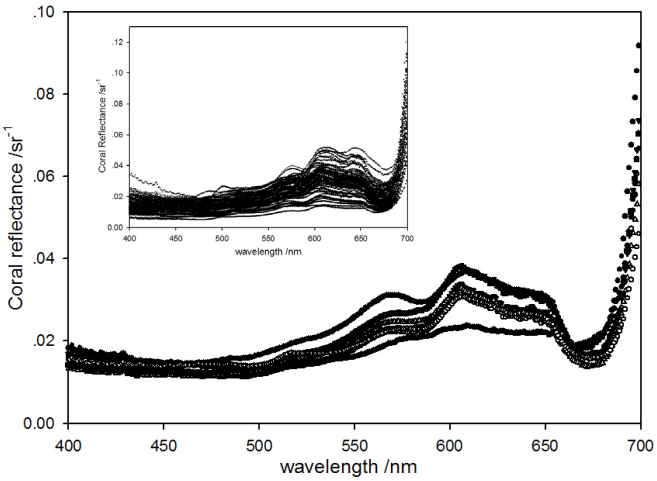

Fig. 5. Coral reflectance plotted against wavelength between 400 and 700 nm.

to a lack of absorbance, and with a pronounced reflectance minimum in the region of 675 nm due to the presence of the photosynthesizing algae (zooxanthellae) within the coral skeleton, rising rapidly beyond 680 nm[13]. The mean zooxanthellae density in these corals of Sanya Bay is ~2.54 × 10^6 cell · cm^{-2}, with *Pavona frondifera* having the lowest (1.39 × 10^6 cell · cm^{-2}) and *Porites lutea* the highest (3.95 × 10^6 cell · cm^{-2})[14]. As fluorescent pigments often occur in corals, and absorb light energy and emit it at less energetic wavelengths, their presence will impact the spectral reflectance.

For coral reef, the peak values vary widely, but the ratios approach to a constant. A peak ratio index (PRI) was proposed here as an indicator to classify coral reef substrates.

$$\frac{R_{\mathrm{rs}}^{2nd} - R_{\mathrm{rs}}^{1st}}{R_{\mathrm{rs}}^{2nd}} = \mathrm{PRI}, \tag{6}$$

where $R^{1\mathrm{st}}{}_{\mathrm{rs}}$ is the reflectance value at the first peak location of the spectral curve; similarly, $R^{2\mathrm{nd}}{}_{\mathrm{rs}}$ is the reflectance value at the second peak location of the spectral curve. We examined spectral shapes by numerically calculating second-derivative spectra following the Savitzky–Golay method[15] and identifying the wavelength locations of local maxima. Figure 6 provides the percentages for each PRI. The most probable values of the index occupy the range from –0.15 to –0.05 (85.8%). For comparison, PRI for sand was also calculated, and has a value of 0.18, –0.038 for seagrass and –8.48 for deep water.

The reflectance of a healthy coral is quite different from that of a non-healthy coral exhibiting a different color. The magnitude and shape of the coral spectra varies with the presence or absence of pigments within the zooxanthellae. Bleached coral has not only a much higher reflectance in general, but also lacks some spectral characteristics of a healthy coral. Spectral derivative analysis was used to identify coral health Fig. 7.

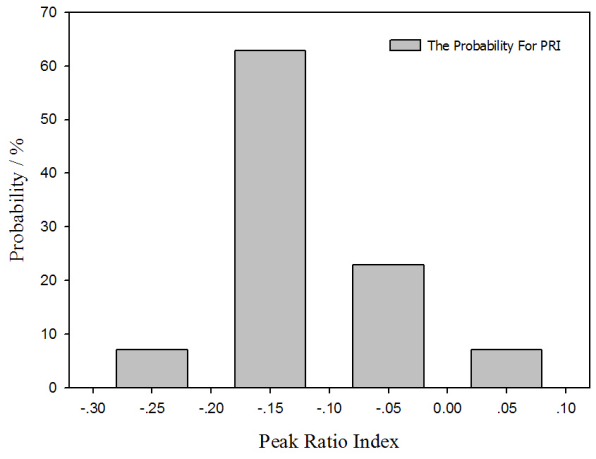

Fig. 6. Vertical bar chart of standardized percentage scores for each PRI, which was calculated based on the coral reflectance in Sanya Bay. The probability of each PRI is expressed as percentage scores.

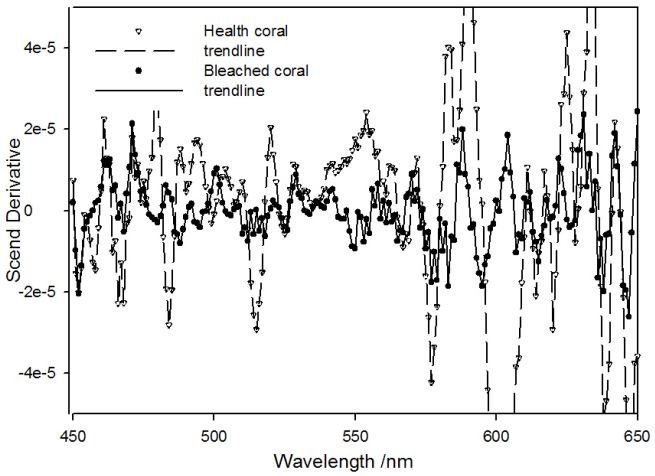

Fig. 7. Second derivative spectra (bottom) of averaged healthy and non-healthy coral spectra.

A positive second derivative at 556 nm was observed for healthy coral, but negative for bleached coral. Among the retrieved spectra, the best discrimination is possible at 556 nm. About 75% of the healthy coral second derivative values at 556 nm were positive, which was validated by in situ visual assessment.

The most obvious trend in the data is that corals exhibit two modes of reflectance. The more common of the two is the triple-peaked pattern because this pattern is expressed by corals that visually appear brown, red, orange, yellow or green, and it is labeled as 'brown coral mode' Fig. 8. Despite variations in magnitude between colonies, the triple-peaked pattern is clearly apparent. In this case, all but a few spectra have very similar values over the range 550–700 nm. The first reflection peak appeared at near 600 nm has a value of about 0.035 sr^{-1}. The depressed reflectance appeared between 400 and 480 nm and by positive reflectance features (i.e., local maxima or shoulders) near 575, 600, and 650 nm.

The less common mode of reflectance visually appeared purple, blue, or pink, and is indicative of

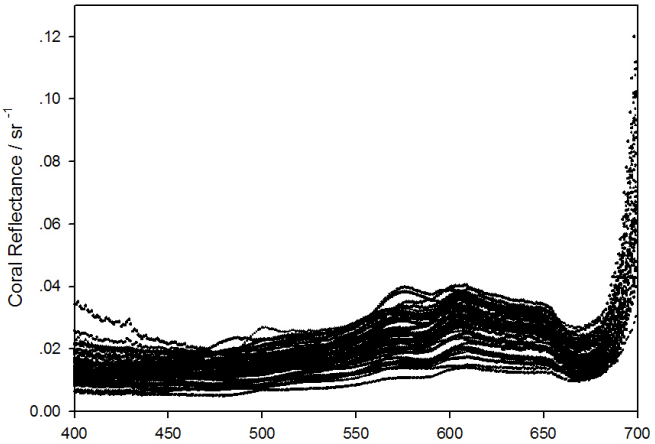

Fig. 8. In situ measured reflectance of Porites colonies plotted against wavelength between 400 and 700 nm.

the possible presence of non-fluorescent proteins, hereafter referred to as 'blue corals' Fig. 9. The reflectance of Acropora is collected (23 coral colonies). Apparent absorption feature can be observed at near 575 nm, leaving a plateau-like shape between 600 and 650 nm. In some colonies, it appears that the 575 nm feature of brown corals (as seen in brown corals) simply has shifted to shorter wavelengths, while in other colonies there is a strong absorption feature in the region. Those corals may contain host pigments which do not fluoresce, but absorb between 560 and 590 nm[16]. The highest variance in reflectance values among viewing angles exists in Acropara due to the structural characteristics of the branching (i.e., sparse nature of the branches and consequent high degree of shadowing[17]). All corals exhibit some degree of variation between reflectance measured at different locations on the colony. So, a greater variation in the Acropora here is likely due to shadows of the branches coupled with the spectrometer FOV, which encompasses variable amounts of branch tips and branch bases. A discernible variation in zooxanthellae density exists among different coral genera in Sanya Bay. Zooxanthellae density in massive Porites (the mean zooxanthellae density in Porites is ~2.54×10^6 cell $\cdot$ cm^{-2}) is higher than that in branching Acropora (~0.67×10^6 cell $\cdot$ cm^{-2})[18]. Ultimately, the variance of Zooxanthellae density contributes to the difference among the spectral reflectance.

Collecting the hyperspectral library and establishing a semi-empirical water column correction model are the crucial steps for hyperspectral analysis of coral reefs. Implementation of the method was found to be effective. The above surface reflectance of coral reef bottom types exhibited a prominent decline at a wavelength longer than 575 nm due to the rapid attenuation of red light in water. Light at the shorter wavelength attenuates lesser than the longer wavelength, and then can penetrate to the greater depth. Within each thin layer of water, a part of the downwelling photons at the water surface get absorbed or get scattered upward as it travels downward to a depth, and so each layer generates an upward flux which undergoes progressive attenuation by absorption and scattering as it travels upward through the water column. For Sanya Bay, the seawater transparence reaches to 6.73 m[19]. For chlorophyll, concentration ranged from 0.30 to 13.58 mg $\times$ m^{-3}, the average concentration and standard deviation (SD) were 1.49 and 1.74 mg $\times$ m^{-3}, respectively[20]. The abundance of *Trichodesmium thiebautii* ranged from 1.14×10^3 to 2060×10^3 trichomes m^{-2}, with an annual mean of 273×10^3 trichomes m^{-2}[21]. Based on the surveys conducted in Sanya Bay, it can be safely concluded that the influence of the water column, especially on the longer wavelength, cannot be ignored, which was validated by the difference between the uncorrected and coral reflectance ($R^2 = 0.05$).

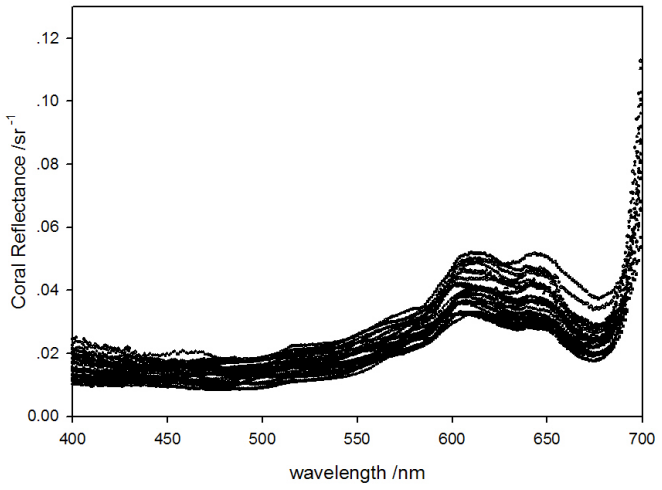

Fig. 9. In situ measured reflectance of Acropora plotted against wavelength between 400 and 700 nm.

In conclusion, the optical model of in-coming solar radiation transfer is applied. Based on the successful algorithm, the hyperspectral library of coral reef is extended for worldwide data collection. The reflectance at 700 nm collected in Sanya Bay is relatively lower than the results conducted by other researchers[13,22]. Reflectance was sensitive to fluctuating light conditions because fluorescence intensity varies with incident irradiance. The maximum irradiance (photosynthetically available radiation) observed in April 11 reached 56 Einstein $\cdot$ m^{-2} day^{-1} in Sanya (18°12′59″ N, 109°28′12″ E; Ocean Level 3 Standard Mapped Image Products in HDF format downloaded from Modis website). Besides, the difference may be related to the absorption and fluorescent properties of zooxanthellae and the zooxanthellae density. In Sanya Bay, zooxanthellae density within the coral reefs span from 0.67×10^6 to 8.48×10^6 cell $\cdot$ cm^{-2}[14]. Zooxanthellae density usually has a greater influence on reflectance than coral morphology. So, different Zooxanthellae densities may be the main reason for the difference. Most probable values of PRI were found to occupy the range from −0.15 to −0.05 (85.8%). About 75% of the healthy coral second derivative values at 556 nm are positive, which is validated by in situ visual assessment. When using the hyperspectral reflectance data set, the most discriminating wavelength subsets at each classification level center on 556, 575, 600 and 650 nm, which can be seen as suitable for classification. And, our results suggest that complete hyperspectral data can be used to conduct coral healthy assessment by allowing the use of derivatives of reflectance. The spectra collected in this study can serve as end members for hyperspectral remote sensing analysis.

This work was supported by the National Basic 973 Program of China (Nos. 2010CB951203 and 2013CB956503), the National Natural Sciences Foundation of China (No. 41176161), the State Oceanic Administration South China Sea Branch Science and

Technology Director Foundation (No. 1338), the State Key Laboratory of Lake Science and Environment (2012SKL004), and the Foundation of Science and Technology of Guangdong Province (No. 2012A031100008).

References

1. D. Yang, and C. Yang, Sensors **9,** 2 (2009).
2. S. L. Liang, Prog. Phys. Geog. **31,** 5 (2007).
3. J. Hedley, C. Roelfsema, and S. Phinn, Remote Sens. Environ. **113,** (2009).
4. L. M. Huang, Y. H. Tan, X. Y. Song, X. P. Huang, H. K. Wang, S. Zhang, J. D. Dong, and R. Y. Chen, Mar. Pollut. Bull. **47,** 1 (2003).
5. Z. P. Lee, K. L. Carder, C. D. Mobley, R. G. Steward, and J. S. Patch, Appl. Opt. **38,** 18 (1999).
6. A. G. Dekker, S. R. Phinn, J. Anstee, P. Bisset, V. E. Brando, B. Casey, P. Fearns, J. Hedley, W. Klonowski, Z. P. Lee, M. Lynch, M. Lyons, C. Mobley, and C. Roelfsema, Limnol. Oceanogr. **1,** 9 (2011).
7. Z. P. Lee, K. L. Carder, and R. G. Steward, J. Geophys. Res. Oceans **110,** C2 (2005).
8. C. Y. Yang, D. T. Yang, W. X. Cao, J. Zhao, G. F. Wang, Z. H. Sun, Z. T. Xu, and M. S. Kumar, R. Int. J. Remote Sens. **31,** 17 (2010).
9. A. Morel and B. Gentili, Appl. Opt. **32,** 33 (1993).
10. A. Morel and L. Prieur, Limnol. Oceanogr. **22,** 4 (1977).
11. M. Chami, D. Mckee, E. Leymarie, and G. Khomenko, Appl. Opt. **45,** 36 (2006).
12. L. G. Henyey and J. L. Greenstein, Astrophys. J. **93,** (1941).
13. H. Holden and E. Ledrew, Int. J. Remote Sens. **20,** 13 (1999).
14. K. F. Yu, Chin. Sci. Bull. **53,** 2 (2008).
15. A. Savitzky and M. J. E. Golay, Anal. Chem. **36,** 8 (1964).
16. C. H. Mazel and E. Fuchs, Limnol. Oceanogr. **48,** 1 (2003).
17. K. E. Joyce and S. R. Phinn, Int. J. Remote Sens. **23,** 2 (2002).
18. S. Li, K. F. Yu, and Q. Shi, Chin. Sci. Bull. **53,** 2 (2008).
19. X. Y. Song, L. M. Huang, Y. H. Tan, J. D. Dong, C. H. Cai, J. L. Zhang, W. H. Zhou, and T. Li, Mar. Sci. Bull. **28,** 6 (2009).
20. C. Y. Shen, P. Shi, Q. G. Xing, S. Z. Liang, M. J. Li, and J. D. Dong, Int. Conf. Geosci. Remote Sens. **2,** 437 (2010).
21. J. D. Dong, Y. Y. Zhang, Y. S. Wang, S. Zhang, and H. K. Wang, Sci. Mar. **72,** 2 (2008).
22. E. J. Hochberg and M. J. Atkinson, Remote Sens. Environ. **85,** 174 (2002).